1-1-2000

Absolute Shape Measurements Using High-Resolution Optoelectronic Holography Methods

Cosme Furlong

Ryszard J. Pryputniewicz
Worcester Polytechnic Institute, rjp@wpi.edu

Absolute shape measurements using high-resolution optoelectronic holography methods

Cosme Furlong
Ryszard J. Pryputniewicz, FELLOW SPIE
CHSLT—Center for Holographic Studies and Laser micro-mechaTronics
Mechanical Engineering Department
Worcester Polytechnic Institute
Worcester, Massachusetts 01609-2280
E-mail: cfurlong@wpi.edu

Abstract. Characterization of surface shape and deformation is of primary importance in a number of testing and metrology applications related to the functionality, performance, and integrity of components. In this paper, a unique, compact, and versatile state-of-the-art fiber-optic-based optoelectronic holography (OEH) methodology is described. This description addresses apparatus and analysis algorithms, especially developed to perform measurements of both absolute surface shape and deformation. The OEH can be arranged in multiple configurations, which include the three-camera, three-illumination, and in-plane speckle correlation setups. With the OEH apparatus and analysis algorithms, absolute shape measurements can be made, using present setup, with a spatial resolution and accuracy of better than 30 and 10 μm, respectively, for volumes characterized by a 300-mm length. Optimizing the experimental setup and incorporating equipment, as it becomes available, having superior capabilities to the ones utilized in the present investigations can further increase resolution and accuracy in the measurements. The particular feature of this methodology is its capability to export the measurements data directly into CAD environments for subsequent processing, analysis, and definition of CAD/CAE models. [S0091-3286(00)02601-5]

Subject terms: CAD/CAE models; fiber optics; optoelectronic holography; shape and deformation measurements; surface tiling.

Paper SM-26 received July 30, 1999; revised manuscript received Aug. 6, 1999; accepted for publication Aug. 6, 1999.

1 Introduction

Characterization of shape and changes in the state of deformation of components is a very important issue in many applications involving concurrent engineering, because these quantities are directly related to the functionality, performance, and integrity of components of interest.[1] Characterization of surface shape can be applied to many areas, which include reverse engineering, quality control, and tribology. Measured shape can be applied to define computer aided design (CAD) models from existing components, so those CAD models can be applied to the computer aided engineering (CAE) analysis or to the manufacturing aspects of existing components. In addition, the measured surface shape can be applied to determine the dimensional accuracy of manufactured components and also to temporally characterize changes in their geometry when subjected to different types of tribological conditions.

Shape and deformation can effectively be determined with quantitative optical techniques, which can provide nondestructive, noninvasive, remote, and full-field-of-view information about the object of interest subjected to realistic loading and boundary conditions.[2,3] For certain applications, determination of surface shape and deformation using the same experimental setup is required. In addition, it is also required that the experimentally obtained data be compatible with other engineering analysis tools, e.g., CAD/CAE software. In the following sections, a unique fiber-optic-based optoelectronic holography (OEH) system capable of providing 3-D surface shape and deformation data compatible with CAD methodologies is described. The OEH system can be arranged in multiple configurations, which include the three-camera, three-illumination, and in-plane speckle correlation. In particular, the procedures and one specific OEH experimental setup utilized to perform surface shape characterization of components are described herein.

2 Description of the OEH System

OEH has been successfully applied to different fields of nondestructive testing of mechanical components.[1,4,5] Being noninvasive and providing qualitative and quantitative full-field information are some of the main advantages of OEH over other experimental techniques. In addition, it requires much less mechanical stability than that required in conventional holographic interferometry. With the OEH, it is possible to perform static and dynamic investigations of mechanical components subjected to a large variety of loading conditions.[1,2,5] Furthermore, it is possible to measure the shape of mechanical components using optical contouring.[1,6] Combination of these capabilities makes the OEH a powerful engineering tool that can be effectively utilized to study and optimize mechanical components.[6] Implementation of recent technological advances in computer and fiber optic technologies to the OEH system has dramatically increased the versatility of the OEH method

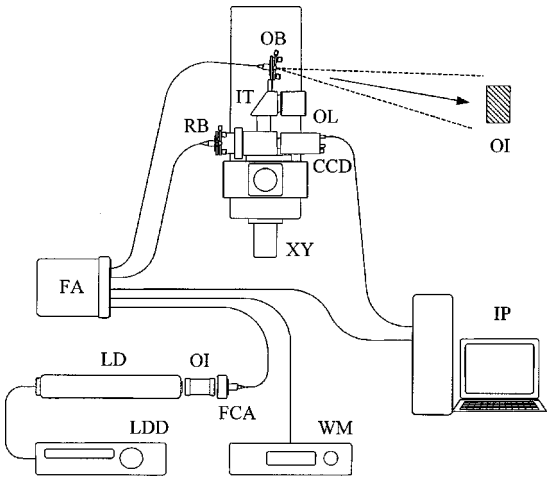

Fig. 1 Fiber-optic-based OEH setup arranged to perform high-resolution surface shape measurements: LDD is the laser diode driver, LD is the laser diode, OI is the optical isolator, FCA is the fiber coupler assembly, WM is the optical wavelength meter, IP is the image-processing computer, FA is the single-mode fiber optic directional coupler assembly, XY is the *X-Y* translational stage, CCD is the CCD camera, RB is the FC-connectorized reference beam, OL is objective lens, OI is the object under investigation, IT is the interferometer, and OB is the FC-connectorized object beam.

and has added the possibility of using it in on-site investigations in order to study and diagnose problems in industrial environments.

2.1 *Experimental Arrangement*

Figures 1–3 depict major components of a currently operational OEH system specifically set up to perform high-resolution surface shape and deformation measurements.[6] The light source is an infrared master-oscillator–power–amplifier (MOPA) laser diode (LD) driven by a controller (LDD), with an operational wavelength centered at 994 nm (at 25°C), capability of wavelength tuning by thermoelectric diode stage cooling, and horizontal linearly polarized output (Fig. 1). The output of the LD is directed through a Faraday optical isolator (OI) providing backreflection isolation to −41 dB at 968 nm. The OI provides 47 deg polarization rotation at 994 nm, and the polarizer on its input

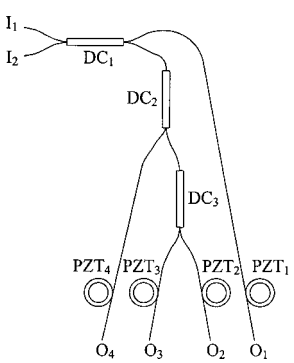

Attenuation, dB

$I_1 - O_1 = 1.10$	$I_2 - O_1 = 1.10$
$I_1 - O_2 = 10.9$	$I_2 - O_2 = 10.9$
$I_1 - O_3 = 10.9$	$I_2 - O_3 = 10.9$
$I_1 - O_4 = 11.7$	$I_2 - O_4 = 11.7$

Splitting, %

I_1	I_2	
80	20	O_1
7	28	O_2
7	28	O_3
6	24	O_4

Fig. 2 Single-mode fiber-optic-based directional coupler assembly (FA in Fig. 1): I_1, I_2 are the FC-connectorized input fibers, DC_1, DC_2, and DC_3 are the directional couplers, PZT_1, PZT_2, PZT_3, and PZT_4 are the ceramic piezoelectric cylinders, and O_1, O_2, O_3, and O_4 are the FC-connectorized output fibers.

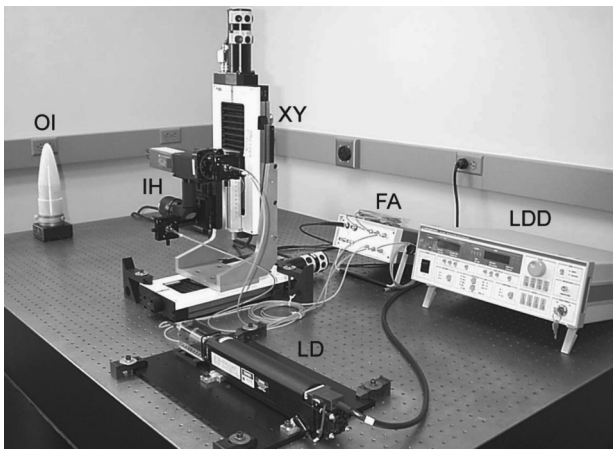

Fig. 3 Fiber-optic-based OEH setup arranged to perform high-resolution surface shape measurements: LD is the laser diode, LDD is the laser diode driver, FA is the single-mode fiber optic directional coupler assembly, XY is the *X-Y* translational stage, IH is the interferometric head, and OI is the object under investigation.

side is set to horizontal principal orientation in order to match the main polarization axis of the LD output. After the OI, light is launched into a single-mode fiber optic directional coupler assembly (FA), Fig. 2, by means of a fiber coupler assembly (FCA), which is composed of a GRIN lens, a five-degree-of-freedom stage, and an FC/AP connector port. The main components of the FA are three single-mode fiber optic directional couplers (DC_1, DC_2, DC_3), four piezoelectric cylinders (PZT_1, PZT_2, PZT_3, PZT_4), and FC-connectorized I/Os. Table 1 summarizes major features of the FA, indicating that the OEH setup can be arranged in the following modes, depending on the experimental requirements:

1. one illumination and three reference beams
2. one reference and three illumination beams
3. four illuminations.

In the experimental arrangement shown in Figs. 1 and 3, the OEH is configured in the mode with one illumination and three reference beams. In this mode, the higher output beam from the FA is utilized as the object beam (OB) to illuminate the object of interest (OI), and one of the lower output beams is used as the reference beam (RB). Object and reference beams are recombined in the interferometer (IT), and the resultant detected irradiances are transmitted to an image-processing computer (IP) through the use of a CCD camera providing video frames with a resolution of 512×480 pixels and digitized to 8 bits. The two additional lower output beams are utilized for monitoring the optical characteristics of the LD. Specifically, one of the lower output beams is utilized as input to the optical wavelength meter (WM), providing absolute wavelength measurements with a resolution of 0.0001 nm, and the additional lower output beam is utilized for monitoring the optical power of the LD. In this experimental configuration, the ceramic piezoelectric cylinder PZT_1 (Fig. 2) is controlled by the IP and used for application of phase-stepping algorithms. In addition, the ceramic piezoelectric cylinder contained in the RB can be utilized for quantitative analysis of time-average

Table 1 Major features of the single-mode fiber optic directional coupler assembly.

Input port	Mode	Application
I_1	One illumination and three reference beams	Three-camera
I_2	One reference and three illumination beams	Three-illumination
I_2	Four illuminations	In-plane speckle correlation

interferograms in situations requiring characterization of both surface shape and dynamically induced deformations.[5,6]

In Figs. 1 and 3, the IT, OB, OL, CCD, RB, and required hardware are mounted on a mechanical fixture (interferometric head, IH), which in turn is assembled onto an X-Y translational stage, with each axis having an independent positioning resolution of 0.1 μm.

The OEH setup shown in Figs. 1–3 uses the two-wavelength technique for generation of interferometric depth contours related to the geometry of the object under investigation.

2.2 *Optical Contouring with the Two-Wavelength Technique*

To determine surface shape using the OEH, the two-wavelength optical contouring technique is applied.[6] The technique is based on the utilization of a coherent and polarized light source with wavelength tuning capabilities. Interferometric depth contours, related to the geometry of the object under investigation, are generated by speckle phase correlation of two sets of phase-stepped speckle intensity patterns, each set acquired at two different wavelengths λ_1 and λ_2.

Phase-stepped speckle intensity patterns are generated by considering the interaction of object and reference beams having complex light fields $F_o(u,v)$ and $F_r(u,v)$, with (u,v) representing the discrete coordinates defining the image plane of the CCD camera. After beamsplitting, and considering the n'th phase step, the detected irradiance resulting from the combined observed and reference-beam irradiances characterized by the wave number $2\pi/\lambda_1$ is described by

$$I_n(u,v)=[F_o(u,v)+F_r(u,v)]\cdot[F_o(u,v)+F_r(u,v)]^* =I_B(u,v)+I_M(u,v)\cos[\Delta\phi(u,v)+\theta_n], \quad (1)$$

where

$$I_B(u,v)=I_o(u,v)+I_r(u,v) \quad (2)$$

is the background irradiance, and

$$I_M(u,v)=2[I_o(u,v)\cdot I_r(u,v)]^{1/2} \quad (3)$$

is the modulation irradiance. In Eqs. (1)–(3), $I_o(u,v)$ and $I_r(u,v)$ are the observed and reference beam irradiances, respectively; $\Delta\phi(u,v)=\phi_o(u,v)-\phi_r(u,v)$, with $\phi_o(u,v)$ representing a random phase due to light scattering from the object of interest and $\phi_r(u,v)$ representing a uniform phase from a smooth reference beam; and θ_n is the imposed n'th known phase step appropriately calibrated for the optical wavelength λ_1. Equations (1)–(3) characterize the acquired first set of phase-stepped speckle intensity patterns.

The second set of phase-stepped speckle intensity patterns is acquired after the wavelength of the LD has been modified to λ_2. Therefore, the detected irradiances resulting from the combined observed and reference-beam irradiances characterized by the wave number $2\pi/\lambda_2$ are described by

$$I'_n(u,v)=I_B(u,v)+I_M(u,v) \times\cos[\Delta\phi(u,v)+\Delta\gamma(u,v)+\theta'_n], \quad (4)$$

where $\Delta\gamma(u,v)$ is the spatial optical phase difference resulting from the change in the wave numbers and related to the absolute shape of the object under investigation, and θ'_n is the imposed n'th known phase step appropriately calibrated for the optical wavelength λ_2. With the OEH, the two sets of phase-stepped speckle intensity patterns are processed in the display and data modes.[2] In the display mode, interference patterns are processed and displayed at video speeds and are modulated by a cosinusoidal function of the form

$$Q_D(u,v)=4I_M(u,v)\cos[\Delta\gamma(u,v)/2] =\{[I_1(u,v)-I_3(u,v)+I'_1(u,v)-I'_3(u,v)]^2 +[I_2(u,v)-I_4(u,v)+I'_2(u,v)-I'_4(u,v)]^2\}^{1/2}, \quad (5)$$

which represents an 8-bit image obtained after applying four phase steps of $\theta_n=\theta'_n=0$, $\pi/2$, π, and $3\pi/2$ to each set of phase-stepped speckle intensity patterns represented by Eqs. (1) and (4). This display mode is used for adjusting, in real time, the contouring parameters for OEH investigations. The data mode is used for performing quantitative investigations.[2,6] In the data mode, additional images are generated: a 16-bit sinusoidal image,

$$N(u,v)=16I_M^2(u,v)\sin\Delta\gamma(u,v) =4\{[I_1(u,v)-I_3(u,v)][I'_2(u,v)-I'_4(u,v)] -[I_2(u,v)-I_4(u,v)][I'_1(u,v)-I'_3(u,v)]\}, \quad (6)$$

and a 16-bit cosinusoidal image,

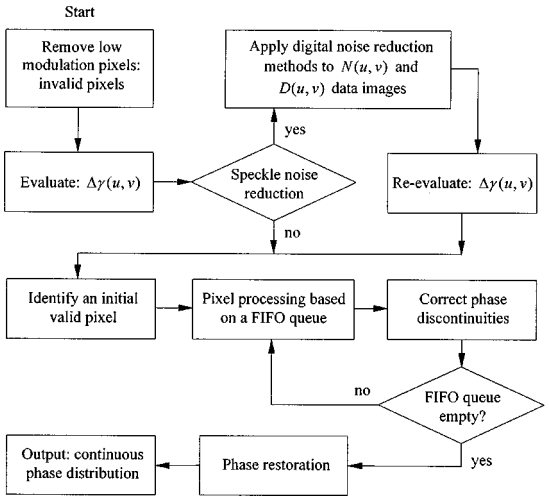

Fig. 4 Flow chart of the phase-unwrapping algorithm applied to processing of $\Delta\gamma(u,v)$ modulo 2π phase maps.

$$D(u,v)=16I_M^2(u,v)\cos\Delta\gamma(u,v)$$
$$=4\{[I_1(u,v)-I_3(u,v)][I_1'(u,v)-I_3'(u,v)]$$
$$+[I_2(u,v)-I_4(u,v)][I_2'(u,v)-I_4'(u,v)]\}, \quad (7)$$

so $\Delta\gamma(u,v)$ can be evaluated using 32-bit arithmetic, as

$$\Delta\gamma(u,v)=\arctan\left[-\frac{N(u,v)}{D(u,v)}\right]$$
$$=\arctan\left[-\frac{(I_1-I_3)(I_2'-I_4')-(I_2-I_4)(I_1'-I_3')}{(I_1-I_3)(I_1'-I_3')+(I_2-I_4)(I_2'-I_4')}\right], \quad (8)$$

where some of the (u,v) arguments have been omitted for clarity. From Eq. (8) it can be observed that the spatial phase distribution represented by $\Delta\gamma(u,v)$ is a discontinuous function wrapped modulo 2π, which must be further processed in order to obtain a continuous spatial phase distribution by application of phase-unwrapping algorithms. The flow chart in Fig. 4 depicts the main procedures of one of the phase-unwrapping algorithms developed[6] for the applications described in this paper. According to Fig. 4, phase unwrapping is initialized by first removing the pixels in the image plane (u,v) containing low-phase-modulation information. Pixels with low modulation, are identified by evaluating $I_M(u,v)$ as

$$I_M(u,v)=(I_1-I_3+I_1'-I_3')^2+(I_2-I_4+I_2'-I_4')^2$$
$$-2[(I_1-I_3)(I_1'-I_3')+(I_2-I_4)(I_2'-I_4')] \quad (9)$$

and by setting a minimum modulation threshold value M_T so that

$$I_M(u,v)<M_T, \quad (10)$$

in which M_T is typically selected as a multiple of the standard deviation of the modulation intensity represented by Eq. (9). Pixels with phase information satisfying the criterion set by Eq. (10) are removed from further processing by application of a binary mask to the data images $N(u,v)$ and $D(u,v)$. Once low-modulation pixels have been removed, $\Delta\gamma(u,v)$ modulo 2π is evaluated, and, depending on the characteristics of the resulting wrapped phase data image, digital speckle noise reduction algorithms may be applied. The phase-unwrapping algorithm continues by selecting a location in the image plane (u_0,v_0) in which to apply the initial condition $\Delta\gamma(u_0,v_0)=\Delta\gamma_0$, around which an unwrapping propagation wavefront based on a first-input, first-output (FIFO) queue develops. At the end of the FIFO queue, phase restoration is applied in order to recover phase information at locations in the image plane (u,v) where low-modulation pixels were initially removed. The result is a continuous spatial phase distribution $\Delta\gamma(u,v)$ related to the absolute shape of the object under investigation.

Determination of the actual absolute shape is performed by mapping the continuous spatial phase distribution data into a domain defined by physical variables of interest. This is accomplished by observing that the optical phase change $\Delta\gamma$ due to a change in wave numbers from $2\pi/\lambda_1$ to $2\pi/\lambda_2$ can be expressed as

$$\Delta\gamma=\frac{2\pi}{\lambda_2}\mathrm{OPL}-\frac{2\pi}{\lambda_1}\mathrm{OPL}=\frac{2\pi}{\Lambda}\mathrm{OPL}, \quad (11)$$

where Λ is the equivalent wavelength given as

$$\Lambda=\frac{\lambda_1\lambda_2}{\lambda_2-\lambda_1}, \quad (12)$$

and OPL is the optical path length defined as the distance from the point of illumination, (x_1,y_1,z_1), to a point on the object of interest, (x_P,y_P,z_P), to the point of observation, (x_2,y_2,z_2). Geometrically, Eq. (11) represents phase contours, which are the result of the intersection of constant optical phase surfaces of revolution with the surface of the object under investigation.

By considering Fig. 5, Eq. (11) can be expressed as

$$\Delta\gamma=\frac{2\pi}{\Lambda}\{[(x_P-x_1)^2+(y_P-y_1)^2$$
$$+(z_P-z_1)^2]^{1/2}+|z_2-z_P|\}, \quad (13)$$

provided that the magnification factors M_u and M_v, which allow the transformation $(M_u u,M_v v)\rightarrow(x_P,y_P)$, are known and a telecentric lens system is used.[6]

Since the image plane (u,v) is parallel to the reference coordinate system (x,y) (Fig. 5) and the magnification factors M_u and M_v can be measured directly using the X-Y translational stage, the only unknown degree of freedom is the surface height represented by the coordinate component z_P, which can be evaluated from Eq. (13) to be

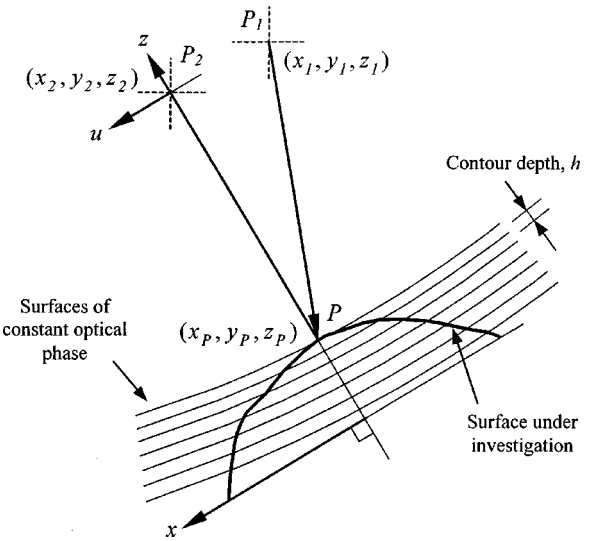

Fig. 5 Geometrical representation of the two-wavelength optical setup used in the determination of surface shape. P_1 is the point of illumination, P_2 is the point of observation, P is a point on the surface under investigation, and the plane (x,y) is parallel to the image plane (u,v).

$$z_P = \frac{1}{2\left[z_1 + \left(\Delta\gamma\frac{\Lambda}{2\pi} - z_2\right)\right]} \times \left[(x_P - x_1)^2 + (y_P - y_1)^2 + z_1^2 - \left(\Delta\gamma\frac{\Lambda}{2\pi} - z_2\right)^2\right]. \tag{14}$$

Determination of surface shape, characterized by the coordinate component z_P, using Eq. (14) requires the knowledge of:

1. The continuous spatial phase distribution $\Delta\gamma$ appropriately transformed from the (u,v) to the (x_P, y_P) domain. This transformation is accomplished by characterization of the magnification factors M_u and M_v.
2. The optical wavelengths λ_1 and λ_2, utilized during the recordings of the two sets of phase-stepped speckle intensity patterns. These parameters are measured directly with an in-line wavelength meter WM (Fig. 1), providing an accuracy of ± 0.0001 nm.
3. The coordinates of the points of illumination, (x_1, y_1, z_1), and observation, (x_2, y_2, z_2). These parameters are obtained by positioning the illumination point (OB, Fig. 1) at a known distance from the point of observation. The point of observation, in turn, is determined by applying camera calibration methods, which provide an accurate position of the optical center C of the imaging system. The point of observation is assigned to the coordinates of C. The camera calibration methods used to characterize the location of C are described in Sec. 2.3.

2.3 *Camera Calibration Methods*

Speckle intensity patterns are acquired with an imaging system containing an array of lenses, which form and project the image of a scene of interest onto the image plane (u,v) located at the CCD of the CCD camera. Therefore, characterization of the properties of the imaging system is necessary in order to quantitatively determine imaging parameters of interest, which facilitate accurate determination of surface shape information from both the continuous spatial phase distribution $\Delta\gamma$ and the illumination-observation geometry characterizing the experimental conditions. Quantitative characterization of the properties of the imaging system is obtained by application of camera calibration methods.[6]

Characterization of the imaging system is accomplished by considering the projection of point P located at the surface of interest, with coordinates $\mathbf{P} = (x,y,z)^T$, onto the point m located on the image plane, with pixel coordinates $\mathbf{m} = (u,v)^T$, as the transformation

$$\begin{pmatrix} U \\ V \\ S \end{pmatrix} = \begin{pmatrix} q_{11} & q_{12} & q_{13} & q_{14} \\ q_{21} & q_{22} & q_{23} & q_{24} \\ q_{31} & q_{32} & q_{33} & q_{34} \end{pmatrix} \begin{pmatrix} x \\ y \\ z \\ 1 \end{pmatrix} = \begin{pmatrix} \mathbf{q}_1^T & q_{14} \\ \mathbf{q}_2^T & q_{24} \\ \mathbf{q}_3^T & q_{34} \end{pmatrix} \begin{pmatrix} \mathbf{P} \\ 1 \end{pmatrix} = \mathbf{Q}\begin{pmatrix} \mathbf{P} \\ 1 \end{pmatrix}, \tag{15}$$

in which

$$u = \frac{U}{S}, \quad v = \frac{V}{S}, \tag{16}$$

are defined by a scalar factor S, for $S \neq 0$, and $\mathbf{Q}$ is the projection perspective matrix.[2,6,7] By application of camera calibration methods, the matrix $\mathbf{Q}$, specifying the transformation from the 3-D space to the 2-D image plane, is determined, and the engineering metrics characterizing the imaging system are extracted from $\mathbf{Q}$.

Determination of the projection perspective matrix $\mathbf{Q}$ is performed by selecting at least 12 i'th points of known coordinates (x_i, y_i, z_i) in a selected 3-D space and, by application of image-processing techniques, identifying their corresponding coordinates (u_i, v_i) in the image plane of the OEH's imaging system. Figure 6 depicts a perspective view of the solid block used for calibration of the OEH's imaging system. The block contains 27 marks of known (x_i, y_i, z_i) coordinates.

With a known set of (x_i, y_i, z_i) coordinates and their corresponding points (u_i, v_i), application of Eqs. (15) and (16) yields

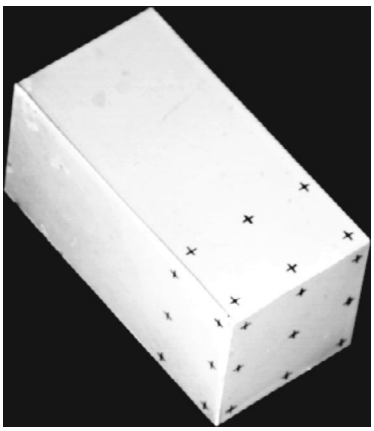

Fig. 6 Solid block, $50\times25\times25\ \text{mm}^3$, used to calibrate the imaging system of an OEH setup. The block contains 27 marks of known (x,y,z) coordinates (centroids).

$$\begin{pmatrix} x_i & y_i & z_i & 1 & 0 & 0 & 0 & 0 & -u_ix_i & -u_iy_i & -u_iz_i & -u_i \\ 0 & 0 & 0 & 0 & x_i & y_i & z_i & 1 & -v_ix_i & -v_iy_i & -v_iz_i & -v_i \\ . & . & . & . & . & . & . & . & . & . & . & . \\ . & . & . & . & . & . & . & . & . & . & . & . \\ . & . & . & . & . & . & . & . & . & . & . & . \end{pmatrix}$$

$$\cdot(q_{11}\ q_{12}\ q_{13}\ q_{14}\ q_{21}\ q_{22}\ q_{23}\ q_{24}\ q_{31}\ q_{32}\ q_{33}\ q_{34})^T=\mathbf{0}, \qquad (17)$$

which is a system of equations of the form $\mathbf{A}\cdot\mathbf{q}=\mathbf{0}$, where $\mathbf{A}$ is a $12\times2M$ matrix of rank 11, with M being the number of calibration points utilized, $\mathbf{q}$ is the unknown vector containing the components of the matrix $\mathbf{Q}$, and $\mathbf{0}$ is the null vector. In order to solve Eq. (17), it is necessary to impose constraints on the system of equations in order to assure that convergence to the trivial solution $\mathbf{q}=\mathbf{0}$, which has no physical significance, is avoided. Constraints are determined from the orthogonality conditions $\|\mathbf{q}_3\|^2=1$ and $(\mathbf{q}_1\times\mathbf{q}_3)\cdot(\mathbf{q}_2\times\mathbf{q}_3)=0$. Once $\mathbf{Q}$ has been calculated by application of constrained optimization methods,[6,8] the optical center C of the imaging system is then evaluated as

$$\begin{pmatrix} x \\ y \\ z \end{pmatrix}_C = \begin{pmatrix} x_2 \\ y_2 \\ z_2 \end{pmatrix} = -\begin{pmatrix} \mathbf{q}_1^T \\ \mathbf{q}_2^T \\ \mathbf{q}_3^T \end{pmatrix}^{-1} \begin{pmatrix} q_{14} \\ q_{24} \\ q_{34} \end{pmatrix}, \qquad (18)$$

which can be applied to Eq. (14) for surface shape measurement.

3 Applications

In this section, the OEH system and analysis algorithms, described in this paper, are utilized as reverse engineering tools with the purpose of facilitating the definition of a CAD model from an existing component, for use in CAE and/or computer-aided manufacturing (CAM) applications.[6]

Figure 7 depicts two samples of the component of interest: a paraboloid of revolution.[2,9] The model is a turned 228.1 ± 0.010-mm-high aluminum piece, specified by three different geometrical sections (as measured with conventional contact techniques): the cylindrical base with diameter 76.12 ± 0.040 mm and height 48.41 ± 0.060 mm, the middle cylindrical section with diameter 69.45 ± 0.040 mm and height 47.49 ± 0.060 mm, and a top parabolic section of specific geometrical characteristics to be determined. It is this parabolic section that is measured using the OEH method.

Fig. 7 Two samples of the paraboloid-of-revolution model. The pieces are 229.0 mm in height with a cylindrical base diameter of 76.12 ± 0.040 mm (as measured with conventional contact techniques). The parabolic section of one of the pieces is to be measured using the OEH method.

3.1 *Experiment Planning: Parameters and Conditions*

Determining the appropriate parameters and conditions before performing a specific shape characterization experiment requires the selection of a feasible measuring resolution and accuracy. The resolution in the measurements is a function of the number of pixels in the CCD camera, as well as of the magnification factors, M_u and M_v, of the imaging system, whereas accuracy in the measurements is a function that depends on:[6]

1. the accuracy to which the continuous spatial phase distribution $\Delta\gamma(u,v)$ is determined, which in turn depends on
   a. the accuracy in the image acquisition process, for which low noise in the CCD camera and relating signal conversion and processing boards are required
   b. the appropriately calibrated phase-stepping algorithm for generation of speckle correlation interferograms and data images
   c. the effective processing of $\Delta\gamma(u,v)$ modulo 2π
2. the magnitude of the equivalent wavelength Λ and its accurate characterization
3. the accurate calibration of the imaging system, which provides imaging metrics that are useful in determining the points of illumination (x_1,y_1,z_1) and observation (x_2,y_2,z_2).

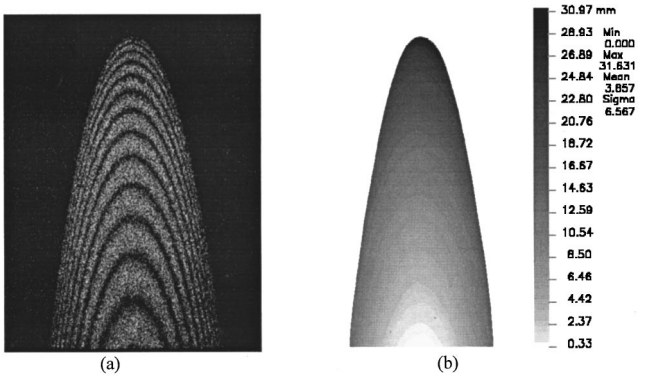

Fig. 8 Measurement of absolute shape: (a) one of the six OEH interferograms obtained at 60-deg increments of the rotational stage, (b) corresponding analysis showing 106,269 pixels with shape information. Camera range 940±3 mm, providing a spatial resolution of 0.1975 mm/pixel and a contour depth uncertainty near 10 μm.

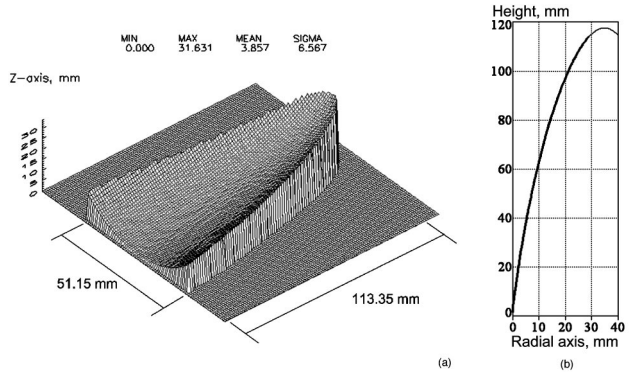

Fig. 9 Measurement of absolute shape: (a) 3-D wire-frame representation obtained by sampling Fig. 8(b) every 6 pixels, (b) measured data points and curve fitting results corresponding to the meridian curve of the paraboloid-of-revolution section. The meridian is defined by a parabolic equation of the form $y=0.1097x^2$ [mm], obtained with a confidence interval near 10 μm.

Once the required resolution and accuracy in the measurements have been selected, the feasible experimental parameters and conditions are determined by minimizing the uncertainty in the contour depth δh, which is related to the accuracy in the measurements. δh is evaluated by considering the contour depth h, obtained from Eq. (14) as the distance corresponding to two consecutive phase contours (Fig. 5) as

$$h=z_{P2}-z_{P1}=h(\Delta\gamma,\Lambda,x_1,y_1,z_1,x_P,y_P,z_2), \tag{19}$$

which indicates that the contour depth is a function of the experimental conditions defining the geometry of the experimental setup: x_1, y_1, z_1, x_P, y_P, z_2, as well as of the experimental parameters $\Delta\gamma$ and Λ. Therefore, δh can be evaluated as

$$\begin{aligned}\delta h=\Bigg[&\left(\frac{\partial h}{\partial(\Delta\gamma)}\delta(\Delta\gamma)\right)^2+\left(\frac{\partial h}{\partial\Lambda}\delta\Lambda\right)^2+\left(\frac{\partial h}{\partial x_1}\delta x_1\right)^2\\&+\left(\frac{\partial h}{\partial y_1}\delta y_1\right)^2+\left(\frac{\partial h}{\partial z_1}\delta z_1\right)^2+\left(\frac{\partial h}{\partial x_P}\delta x_P\right)^2\\&+\left(\frac{\partial h}{\partial y_P}\delta y_P\right)^2+\left(\frac{\partial h}{\partial z_2}\delta z_2\right)^2\Bigg]^{1/2},\end{aligned} \tag{20}$$

in which $\delta(\Delta\gamma)$, δx_1, δy_1, δz_1, δx_P, δy_P, δz_2 are the uncertainties in the corresponding variables, and $\delta\Lambda$ is the uncertainty in the equivalent wavelength Λ, given as

$$\delta\Lambda=\left[\left(\frac{\partial\Lambda}{\partial\lambda_1}\delta\lambda_1\right)^2+\left(\frac{\partial\Lambda}{\partial\lambda_2}\delta\lambda_2\right)^2\right]^{1/2}. \tag{21}$$

3.2 *Representative Measurements*

Figure 3 depicts the experimental arrangement with the object of interest mounted on a 1/60-deg resolution rotational stage and positioned at 940±3-mm camera range.[6] A full rotational section of the sample is measured at a constant y position of the X-Y translational stages using six 60-deg rotational stage increments. Figures 8–10 show typical results obtained after measuring a full rotational section of 113.35 mm in height. Figure 8 depicts one of the six interferograms and the corresponding analysis results, illustrating a 2-D representation of the measurements containing 106,269 pixels with shape information at a resolution of 0.1975 mm/pixel and a contour depth uncertainty, related to the accuracy in the measurements, near 10 μm. Figure 9(a) depicts a 3-D wire-frame representation of the shape analysis obtained by sampling Fig. 8(b) every 6 pixels, while Fig. 9(b) shows the measured data points as well as curve-fitting results corresponding to the meridian curve of the paraboloid-of-revolution section. Curve-fitting results indicate that the meridian is defined by a parabolic equation of the form $y=0.1097x^2$, obtained with a confidence interval within the uncertainty in the measurements.

The (x,y,z) data clouds obtained from every 60-deg section can be imported into a CAD environment[10] for further processing and analysis (Fig. 10). The process by which a single geometrical CAD surface is assembled from individual (x,y,z) data clouds is known as *tiling*. Tiling is a

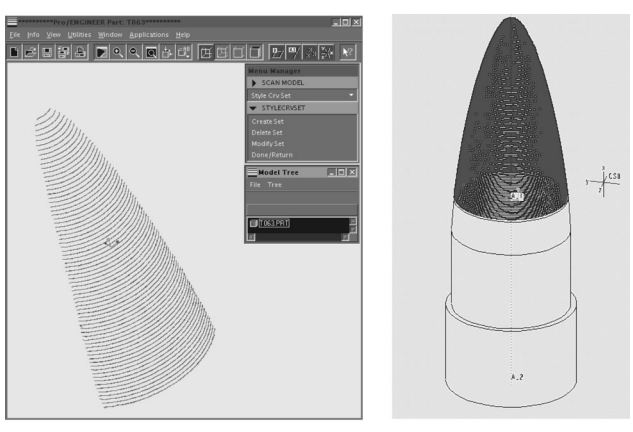

Fig. 10 Measurement of absolute shape: subsampled (x,y,z) data clouds of measured sections imported into a CAD environment (Pro/Engineer); (a) single section and (b) tiled sections used for defining the geometry of the entire component.

current CAD problem that requires further investigations, which could guarantee the generation of an accurate single geometrical CAD surface representation.

4 Conclusions and Recommendations

An OEH system arranged in a one-camera configuration to perform optical contouring using the two-wavelength technique has been presented. Representative measurements shown provide a spatial resolution of 197.5 μm and an accuracy near 10 μm at 940 ± 3-mm camera range, which are considered sufficient for reverse-engineering purposes. Resolution can be increased by changing the camera range, using a different lens system, or using a denser CCD array, whereas accuracy can be increased by using smaller contour depths, which requires a wide-range tunable laser. Accuracies of better than 10 μm can be achieved for wavelengths characterized with an accuracy of 0.0001 nm, an equivalent wavelength Λ of 2 mm, a camera range of 750 mm, an imaging system calibrated to within 5% uncertainty, and $\Delta\gamma$ determined to within 5% uncertainty. Further developments include the implementation of a fully automatic OEH shape-measuring system, which may require the incorporation of a more suitable tunable light source and an image-processing system with better capabilities than the ones utilized in the present investigations. In addition, further investigations pertaining to surface tiling of different range views are required in order to obtain an accurately defined CAD model.

Acknowledgments

The authors would like to thank all members of the CHSLT for their helpful discussions and assistance during preparation of this paper.

References

1. C. Furlong and R. J. Pryputniewicz, ''Hybrid computational and experimental approach for the study and optimization of mechanical components,'' *Opt. Eng.* **37**(5), 1448–1455 (1998).
2. R. J. Pryputniewicz, *Holographic Numerical Analysis*, Center for Holographic Studies and Laser micro-mechaTronics, Mechanical Engineering Department, Worcester Polytechnic Institute, Worcester, MA (1992).
3. C. M. Vest, *Holographic Interferometry*, Wiley, New York (1979).
4. K. A. Stetson and W. R. Brohinsky, ''Electro-optic holography system for vibration analysis and nondestructive testing,'' *Opt. Eng.* **26**(12), 1234–1239 (1987).
5. R. J. Pryputniewicz and K. A. Stetson, ''Measurement of vibration patterns using electro-optic holography,'' *Proc. SPIE* **1162**, 456–467 (1989).
6. C. Furlong, ''Hybrid, experimental and computational, approach for the efficient study and optimization of mechanical and electromechanical components,'' PhD Dissertation, Worcester Polytechnic Institute, Worcester, MA (1999).
7. O. D. Faugeras, T. Luong, and S. Maybank, ''Camera self-calibration: theory and experiments,'' in *Proc. 2nd European Conf. in Computer Vision*, G. Sandini, Ed., pp. 321–334, Springer-Verlag, Berlin (1992).
8. G. H. Golub and C. F. Van Loan, *Matrix Computations*, The Johns Hopkins University Press, Baltimore (1991).
9. R. J. Pryputniewicz, ''Holographic analysis of body deformations,'' Ph.D. Dissertation, University of Connecticut, Storrs, CT (1976).
10. Pro/Engineer, *Pro/Scan-Tools. User's Guide v. 20.0*, Parametric Technology Corporation, Waltham, MA (1999).

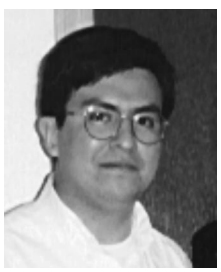

Cosme Furlong obtained his Mechanical Engineering degree from the University of the Americas (Mexico) in 1989, and his MS and PhD in mechanical engineering from Worcester Polytechnic Institute (WPI), Worcester, Massachusetts, in 1992 and 1999, respectively. He is currently at the WPI/ME—CHSLT. His professional interests include the combined use of modeling and simulation with quantitative optical techniques, fiber optics, optoelectronic holography, nondestructive testing, image processing, numerical analysis, materials characterization, and optimization of mechanical and electromechanical components.

Ryszard J. Pryputniewicz: Biography appears with the paper "New test methodology for static and dynamic shape measurements of microelectromechanical systems," in this issue.